Research Paper

Open-Switch Fault Tolerance Strategy for Induction Motor Drive System

*Hicham Zaimen[1, *] [iD] , Ali Rezig[1], and S. Touati[2]*

[1] L2EI Laboratory, Jijel University, BP 98 Ouled Aïssa 18000, Jijel, Algeria.

[2] Electrical Engineering Department, Nuclear Research Center of Birine, CRNB Bp 180, Ain Oussera, Algeria.

Abstract— *Voltage source inverters (VSIs) based on insulated-gate bipolar transistors (IGBTs) may face various faults that can affect the operation and safety of the entire electric drive system. To enhance the reliability of the drive system, it is crucial to develop an accurate fault diagnosis (FD) method and increase fault tolerance control (FTC) capabilities. This paper provides a novel FTC strategy for IGBT open circuit fault (OCF) in induction motor (IM) drives. The proposed FTC strategy includes a fault diagnosis algorithm and inverter reconfiguration. A three-phase current-based diagnosis method (FD) is adopted in this research, where the average absolute value of the normalized currents is used to extract fault detection variables. The developed FD method does not need any extra sensors and provides fast diagnosis time, which is equivalent to almost 25-30% of the phase current's fundamental cycle. To accomplish satisfactory post-fault operation of the IM drive, a four-leg inverter topology is employed. Finally, the effectiveness of the proposed fault-tolerant drive and diagnosis method is proven through various simulation results.*

Keywords— Voltage source inverter, open switch faults, fault diagnosis, indirect field-oriented control, induction motor drives, fault-tolerant control.

1. INTRODUCTION

Three-phase induction motor drives (IMDs) are widely used in industrial processes. These IMDs are known for their advantages, such as simplicity, reduced maintenance, improved robustness, and cost, compared to DC motors [1]. Nevertheless, these drives may face various faulty conditions, such as failures of VSI power switches, sensor faults, and machine faults. Thus, there is an increasing demand nowadays regarding the safety and reliability of electrical drive systems, especially for critical applications such as electric vehicles, nuclear power, medical equipment, aerospace, and so on. Therefore, fault diagnosis and FTC are helpful to enhance the reliability of the drive systems.

Mostly, induction motors (IMs) are powered by voltage-source inverters. Due to continuous operation, these VSIs can be subject to various fault modes. The most common faults are short-circuit (SC) and open-circuit (OC) faults in power semiconductor devices. Statistical data mentioned that almost 38% of drive system faults are due to power switch device failures [2]. The SC faults occur quickly and have serious effects, so it is difficult to achieve fault diagnostic (FD) and fault tolerance (FT) strategies. However, SC faults can be converted into OC faults by using a fast scorcher in the VSI [3]. One main component of VSI is the insulated gate bipolar transistor (IGBT) device, known for its ability to handle high voltages and currents while providing fast switching speeds. The IGBT open circuit faults (OCFs) do not immediately shut down the drive system, but they can degrade the output quality of the VSI and stress other system parts, which could lead to more failures. Over time, OCF can prompt a total system shutdown [4]. To overcome this issue, this paper aims to develop fault diagnosis and FTC systems that can bypass the IGBT open-circuit faults (OCFs).

Over the years, numerous diagnostic techniques have been proposed in the literature for AC motor drives [5]. These techniques can be classified according to easily accessible signals, namely current signals (current-based techniques) and voltage signals (voltage-based techniques) [6]. The voltage-based approaches present features such as high immunity to false alarms and fast diagnosis speed, but they often need extra sensors, so the implementation cost is high. Unlike voltage approaches, current-based ones are broadly employed thanks to their advantages, such as avoiding the use of additional sensors and easily embedding them into existing control algorithms [7]. The current-based methods are the most popular. The following includes a review of some current-based methods. In [8], a Park's vector method is proposed, where the diagnosis process is done by computing the average value of Park's vector current. The main weakness of this approach is its load dependency. To overcome the issue of load dependency, the DC-normalized current method is proposed in [9, 10]. This method has some demerits in the case of closed-loop control systems. In [11], a diagnosis method based on the current-vector trajectory diameter was proposed. The major drawbacks of this method are load dependency and slow detection. In [12], the single and multiple OCFs are diagnosed through the error between measured currents and their references. This method is unsuitable for open-loop control strategies such as V/f scalar control. Other current-based methods are the average absolute values of phase currents [13] and current slope [14].

These methods are simple to implement but may produce false alarms under load and speed transients.

The method in Ref. [13] has been improved later through a fuzzy logic (FL) approach [15, 16]. The reference [17] proposes a diagnosis approach for permanent magnet synchronous motor (PMSM) drives. This latter avoids using additional sensors and can detect all VSI OCFs, but its fault detection time is too long. In [18], the authors propose a new method based on the reconstruction of phase currents using a single DC-current sensor. This method can diagnose single OCFs and part of double OCFs. The only drawback to this method is the long detection time, which is about one current cycle. More recently, other diagnosis methods were discussed, such as in [19–22]. These FD methods possess fast detection capability, but either use multiple diagnosis variables or need to set thresholds for accurate diagnosis.

As mentioned earlier, to ensure the reliable and safe operation of the IMDs after the OCF diagnosis process, the fault-tolerant control system must be activated, particularly in safety-critical industrial systems where uninterrupted operation is obligatory, and poor operation performance cannot be accepted [23]. These FTC methods integrate FD algorithms and hardware or software redundancy, allowing correct drive operation under faulty conditions. Several fault tolerance strategies have been addressed in the literature for AC drives in recent years. In Refs. [24, 25], the authors proposed an FTC method against open-phase faults (OPF) based on both a modified vector control strategy and VSI reconfiguration. One of its drawbacks is the need for a motor neutral point, which makes it suitable only for Y-connected motors. In addition, this FTC method does not include the FD process. The authors of [19, 26] proposed a fault tolerance strategy based on a four-switch three-phase VSI. This strategy is suitable for star or delta-connected motors but is limited to low-speed applications.

This paper proposes a new fault-tolerant control system for vector-controlled induction motors that deals with VSI open-circuit faults. The FTC system can first detect and identify the faulty switch using a motor current-based diagnostic method. The next step is the isolation of the VSI faulted leg and replace it with a redundant leg. In this case, the fault-tolerant VSI topology is called the four-leg VSI topology. The contributions of this research are as follows:

- The FD method is based on the signal characteristics of measured currents and avoids using additional measurement devices. Thus, the cost of the fault-tolerant control system will be lower.
- Besides, most of the diagnostic approaches for VSI OCFs are based on at least two diagnosis variables and require the selection of detection thresholds. In contrast, the proposed FD method uses a single diagnosis variable and an adaptive threshold. Hence, the diagnosis algorithm is greatly simplified.
- In several previous works concerned with three-phase AC drives, the FTC methods require both a change in the control strategy of the VSI and its topology. The presented FTC method avoids the change in the VSI controller.

The remainder of this paper is structured as follows: The fault diagnosis method and fault tolerance strategy for open-switch faults are presented in Section 2 and Section 3, respectively. Section 4 presents the simulation results obtained from MATLAB/SIMULINK. Finally, the conclusions and future topics are summarized in Section 5.

2. PROPOSED FAULT DIAGNOSIS METHOD

2.1. System description of induction motor drive

Fig. 1 shows a control block diagram of the IM drive system, which includes a two-level VSI, an induction motor, a space vector modulation (SVM)-based indirect field-oriented controller (IFOC), and sensors for phase currents and position.

where T_1 to T_6 are IGBTs with anti-parallel diodes, i_a, i_b, i_c are three-phase currents, and U_{dc} represents the dc-link voltage. The IGBT switches are controlled using an SVM algorithm.

Defining the switching function $S_i(i = 1, 3, 5)$ as:

$$S_i|_{i=1,3,5} = \begin{cases} 1, & T_i \text{ is ON, } T_{i+1} \text{ is OFF} \\ 0, & T_i \text{ is OFF, } T_{i+1} \text{ is ON} \end{cases} . \quad (1)$$
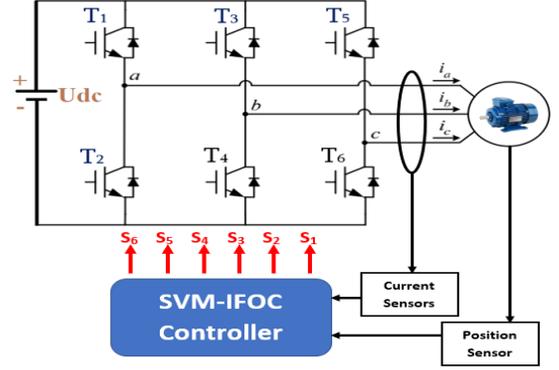

Fig. 1. Control block diagram of the IM drive system.

Under normal conditions, the phase voltages $Vx(x = a, b, c)$ can be expressed as a function of the switching signals of the upper IGBTs (S_1, S_3, S_5) as follows:

$$\begin{bmatrix} Va \\ Vb \\ Vc \end{bmatrix} = \frac{U_{dc}}{3} \begin{bmatrix} 2 & -1 & -1 \\ 1 & 2 & -1 \\ -1 & -1 & 2 \end{bmatrix} \begin{bmatrix} S_1 \\ S_3 \\ S_5 \end{bmatrix} . \quad (2)$$

2.2. Phase currents analysis under IGBTs open circuit faults

In this paper, a total of nine OC fault conditions will be considered for the power switches, including six single open-switch faults and three open-phase faults (double-switch in the same leg). Assumed that the IM is supplied with a fault-free VSI. During one-cycle T, the IM phase currents will be pure sin waves, which are represented by Eq. (3) [5]:

$$\begin{cases} i_a(t) = I_P \sin(\omega_e t) \\ i_b(t) = I_P \sin(\omega_e t - 2\pi/3) \\ i_c(t) = I_P \sin(\omega_e t + 2\pi/3) \end{cases} , \quad t \in [0, T]. \quad (3)$$

where Ip is the current amplitude and ω_e is the angular frequency of currents.

A) Single open-switch fault analysis

Case 1: when an OCF affects an upper IGBT (e.g., T_3 of b-phase), the b-phase current i_b drops to zero through the positive half-cycle and is expressed as:

$$i_b(t) = \begin{cases} 0 & t \in [T/3, 5T/6] \\ I_P \sin(\omega_e t - 2\pi/3) & t \in [0, T/3] \ \& \ [5T/6, T] \end{cases} \quad (4)$$

$$i_b(t) = \begin{cases} 0 & t \in [T/3, 5T/6] \\ I_P \sin(\omega_e t - 2\pi/3) & \begin{array}{l} t \in [0, T/3], \\ \text{and } t \in [5T/6, T] \end{array} \end{cases} .$$

Case 2: a lower IGBT is subjected to OCF (e.g., T_2 of a-phase). Thus, the current i_a becomes zero in the negative half-period and is given as:

$$i_a(t) = \begin{cases} I_P \sin(\omega_e t) & \text{for } t \in [0, T/2] \\ 0 & \text{for } t \in [T/2, T] \end{cases} . \quad (5)$$

In the two above cases, the remaining phase currents for healthy legs will be distorted to maintain Eq. (6) [17]:

$$i_a + i_b + i_c = 0. \quad (6)$$

B) Open-phase faults analysis

In this case, OCF occurs in two IGBTs of the same leg. For instance, the IGBT (T_1, T_2) of the a-phase are in OCF simultaneously. As a result, both the negative and positive half cycles of the a-phase current i_a are lost, so the current i_a becomes zero. As the IM is considered a balanced load, the phase currents in the two remaining phases assume opposite-phase signals and their amplitudes increase by a factor of $\sqrt{3}$. The current formulas, in this case, are given by [1, 17]:

$$\begin{aligned} i_a(t) &= 0 \\ i_b(t) &= I_P \sqrt{3}\left[\sin(\omega_e t - 2\pi/3) + 1/2\sin(\omega_e t)\right] \\ i_c(t) &= -I_P \sqrt{3}\left[\sin(\omega_e t + 2\pi/3) - 1/2\sin(\omega_e t)\right] \end{aligned} \quad (7)$$

for

$$t \in [0, T]$$

2.3. Design of IGBT open-circuit faults diagnosis method

Based on the previous discussion of the different VSI OCF features, only the three-phase currents (i_{abc}) are needed in the proposed OCF diagnosis method. Hence, the fault diagnostic process does not require additional measurement devices and is easily integrated with the SVM-IFOC controller. Additionally, the proposed FD method uses only one fault diagnosis variable ηx ($x = a, b, c$) to achieve faulty switch detection and identification. Each diagnostic variable ηx includes two fault indicators; the first one is the average absolute value of the subtraction of two normalized line currents $\langle |I_x^N| \rangle$, while the other is the average value of the normalized currents $\langle i_x^N \rangle$. The variables ηx are expressed as follows:

$$\begin{cases} \eta_a = \dfrac{\langle |I_a^N| \rangle - \delta}{\langle i_b^N \rangle + \langle i_c^N \rangle + 1}, \ \eta_b = \dfrac{\langle |I_b^N| \rangle - \delta}{\langle i_c^N \rangle + \langle i_a^N \rangle + 1} \\ \eta_c = \dfrac{\langle |I_c^N| \rangle - \delta}{\langle i_a^N \rangle + \langle i_b^N \rangle + 1}, \ \delta = 2\sqrt{2}/\pi \end{cases} \quad (8)$$

where the normalized line-line currents $\left(I_x^N\right)$ are described as follows [5]:

$$I_x^N\Big|_{x=a,b,c} = \begin{cases} I_a^N = i_b^N - i_c^N = -\sqrt{2}\cos(\omega_e t) \\ I_b^N = i_c^N - i_a^N = +\sqrt{2}\cos(\omega_e t + \pi/3) \\ I_c^N = i_a^N - i_b^N = +\sqrt{2}\cos(\omega_e t - \pi/3) \end{cases} \quad (9)$$

To make the FD algorithm insensitive to load, the phase currents should be normalized as follows:

$$i_x^N = \frac{i_x}{|i_{\alpha\beta}| + \varepsilon} = \begin{cases} i_a^N = \sqrt{2/3}\sin(\omega_e t) \\ i_b^N = \sqrt{2/3}\sin(\omega_e t - 2\pi/3) \\ i_c^N = \sqrt{2/3}\sin(\omega_e t + 2\pi/3) \end{cases} \quad (10)$$

where ε is a very small positive quantity and $|i_{\alpha\beta}|$ denotes the Park's vector modulus given in Eq. (11) [5]:

$$|i_{\alpha\beta}| = \sqrt{i_\alpha^2 + i_\beta^2} = I_P \sqrt{3/2}. \quad (11)$$

Here, i_α and i_β are the current components in the stationary $\alpha\beta$-plane. According to Eq. (10), the normalized currents always assume values in the range of $\pm\sqrt{2/3}$.

The average values of the normalized currents $\langle i_x^N \rangle$ are written as follows:

$$\langle i_x^N \rangle = \frac{1}{T}\int_0^T i_x^N \, dt, \ x \in \{a, b, c\} \quad (12)$$

where $< >$ is the signal average value at the fundamental frequency.

The variable $\langle i_x^N \rangle$ has four possible values. It is 0 for a healthy operation or when OCF occurs in two switches of the same leg (open-phase fault). In healthy VSI operations, the three diagnostic variables given in Eq. (8) are:

$$\eta_a = \eta_b = \eta_c = 0. \quad (13)$$

In the event of a single IGBT OCF, the average values $\langle i_b^N \rangle$ and $\langle i_a^N \rangle$ over one cycle T are expressed in Eqs. (14) and (15), respectively:

$$\begin{aligned} \langle i_b^N(t) \rangle &= \tfrac{1}{T}\int_0^{T/3}\sqrt{2/3}\sin(\omega_e t - 2\pi/3)dt + \\ &\tfrac{1}{T}\int_{5T/6}^{T}\sqrt{2/3}\sin(\omega_e t - 2\pi/3)\,dt = -\sqrt{6}/3\pi \end{aligned} \quad (14)$$

$$\langle i_a^N(t) \rangle = \frac{1}{T}\int_0^{T/2}\sqrt{2/3}\sin(\omega_e t)\,dt = \sqrt{6}\big/3\pi \quad (15)$$

Thus, the average values of the normalized motor's currents can be written as follows:

$$\langle i_x^N \rangle = \begin{cases} 0 & \text{if normal and OPF conditions} \\ -\sqrt{6}/3\pi & \text{if OCF in } T_i\ (i = 1, 3, 5) \\ +\sqrt{6}/3\pi & \text{if OCF in } T_j\ (j = 2, 4, 6) \end{cases}, \ x \in \{a, b, c\} \quad (16)$$

Next, the absolute value of normalized line-line currents $|I_x^N|$ under healthy VSI conditions are given as follows:

$$|I_a^N(t)| = \begin{cases} +\sqrt{2}\cos(\omega_e t) & \text{for } t \in [0, T/4] \\ -\sqrt{2}\cos(\omega_e t) & \text{for } t \in [T/4, 3T/4] \\ +\sqrt{2}\cos(\omega_e t) & \text{for } t \in [3T/4, T] \end{cases} \quad (17)$$

$$|I_b^N(t)| = \begin{cases} +\sqrt{2}\cos(\omega_e t + \pi/3) & \text{for } t \in [0, T/12] \\ -\sqrt{2}\cos(\omega_e t + \pi/3) & \text{for } t \in [T/12, 7T/12] \\ +\sqrt{2}\cos(\omega_e t + \pi/3) & \text{for } t \in [7T/12, T] \end{cases} \quad (18)$$

$$|I_c^N(t)| = \begin{cases} +\sqrt{2}\cos(\omega_e t - \pi/3) & \text{for } t \in [0, 5T/12] \\ -\sqrt{2}\cos(\omega_e t - \pi/3) & \text{for } t \in [5T/12, T] \end{cases} \quad (19)$$

For example, the average absolute value $\langle |I_a^N| \rangle$ over one cycle T can be expressed as:

$$\begin{aligned} \langle |I_a^N(t)| \rangle &= \tfrac{1}{T}\int_0^{T/4} +\sqrt{2}\cos(\omega_e t)\,\partial t + \\ &\tfrac{1}{T}\int_{T/4}^{3T/4} -\sqrt{2}\cos(\omega_e t)\,\partial t + \\ &\tfrac{1}{T}\int_{3T/4}^{T} +\sqrt{2}\cos(\omega_e t)\,\partial t = 2\sqrt{2}/\pi \end{aligned} \quad (20)$$

Table 1. Average absolute values of I_x^N for different OCFs.

Types of OC faults	Average absolute values		
	$\langle|I_a^N|\rangle$	$\langle|I_b^N|\rangle$	$\langle|I_c^N|\rangle$
T1	1.15	0.8	0.8
T2	1.15	0.8	0.8
T3	0.8	1.15	0.8
T4	0.8	1.15	0.8
T5	0.8	0.8	1.15
T6	0.8	0.8	1.15
T1 & T2	1.4	0.7	0.7
T3 & T4	0.7	1.4	0.7
T5 & T6	0.7	0.7	1.4

Table 2. Diagnosis signatures for power switch open circuit faults.

State	Faulty switch	Diagnosis variables and flags					
		η_a	η_b	η_c	$IGBT_{12}$	$IGBT_{34}$	$IGBT_{56}$
Single open switch	T_1	P_1	N	N	1	0	0
	T_2	P_2	N	N	-1	0	0
	T_3	N	P_1	N	0	1	0
	T_4	N	P_2	N	0	-1	0
	T_5	N	N	P_1	0	0	1
	T_6	N	N	P_2	0	0	-1
Double-switch	T_1 & T_2	P_3	N	N	2	0	0
	T_3 & T_4	N	P_3	N	0	2	0
	T_5 & T_6	N	N	P_3	0	0	2
Normal	-	Z	Z	Z	0	0	0

The same analysis as in Eq. (20) is applied for I_b^N and I_c^N. Thus, under the normal operation of the VSI, the value of $\langle|I_x^N|\rangle$ is given as:

$$\langle|I_x^N|\rangle = \delta = 2\sqrt{2}/\pi \approx 0.9 \tag{21}$$

The approximate values of $\langle|I_x^N|\rangle$ for a single-switch OC fault and a double-switch OC fault are listed in Table 1 [5].

It has been shown through calculations that when an OCF happens in an upper switch (i.e., T_1, T_3, T_5), the corresponding diagnostic variable ηx rises quickly to 0.2, while for bottom switch OCFs (i.e., T_2, T_4, T_6), it rises to 0.34. In addition, when an open-circuit fault happens in both switches T_i and T_{i+1} ($i = 1, 3, 5$) of the same leg, the corresponding variable ηx converges to 0.5. Otherwise, the diagnosis variable ηx is near 0 under normal conditions. By comparing the variables ηx to an adaptive threshold Th_{ad}, the detection and localization processes of different OCF scenarios are performed as follows:

$$\eta_x|_{x=a,b,c} = \begin{cases} N & \text{if } \eta_x < 0 \\ P_1 & \text{if } Th_{ad} \leq \eta_x < 0.2 \\ P_2 & \text{if } Th_{ad} \leq \eta_x < 0.34 \\ P_3 & \text{if } Th_{ad} \leq \eta_x < 0.5 \\ Z & \text{if } \eta_x = 0 \end{cases} \tag{22}$$

According to Eq. (22), Z indicates normal operation, P_1 indicates an upper switch OCF, P_2 indicates a lower switch OCF, and P_3 means that OCF happens in two IGBTs of the same leg.

The selection of a good threshold value is important for fault diagnosis robustness. If the fixed threshold value is high or low, the fault sensitivity is reduced, or the false alarm rate is increased, respectively [27]. Therefore, an adaptive threshold Th_{ad} is adopted in this paper, which is defined as follows:

$$\begin{cases} Th_{ad} = 0.5\left(\eta_{\text{Max}} + \eta_{\text{Min}}\right) \\ \eta_{\text{Max}} = \text{Max}\left(\eta_a, \eta_b, \eta_c\right), \ \eta_{\text{Min}} = \text{Min}\left(\eta_a, \eta_b, \eta_c\right) \end{cases} \tag{23}$$

Define $IGBT_{ij}$ as the fault diagnostic flags expressed as follows:

$$IGBT_{ij} = \begin{cases} 1 & \text{OCF in } T_i \\ -1 & \text{OCF in } T_j \\ 2 & \text{OCF in } T_i \ \& \ T_j \end{cases} \quad \begin{matrix} i = 1, 3, 5 \\ j = i + 1 \end{matrix} \tag{24}$$

Through the above analysis, by using the diagnostic variables ηx and flags $IGBT_{ij}$, the OCF diagnosis signatures are displayed in Table 2.

Fig. 2 describes the schematic diagram of the suggested FD method. The inputs of the diagnosis algorithm are the measured currents i_x ($x = a, b, c$), and the outputs are the faulty switches T_{if} ($i = 1 : 6$).
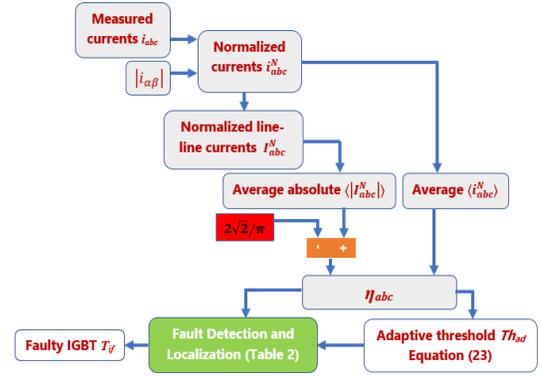

Fig. 2. Schematic diagram of the IGBT OCF diagnosis method.

3. OPEN SWITCH FAULT-TOLERANT CONTROL STRATEGY

To provide fault-tolerant capability in the case of an IGBT open circuit fault as well as increase the reliability of the induction motor system, a fault-tolerance control FTC strategy is proposed. This strategy relies on the modification of the conventional three-leg VSI topology. Based on the principle of redundancy, a fourth leg (r-leg) consisting of two power switches (T_7, T_8) is added to three phase VSI and permanently connected to each phase through the corresponding bidirectional switch TRIACs (TRa, TRb, or TRc) as illustrated in Fig. 3 [28]. The Ka, Kb, and Kc are the isolation switches of the faulty leg.
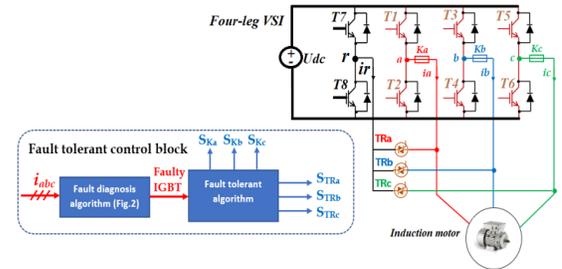

Fig. 3. Proposed fault-tolerant control strategy based on four legs VSI topology.

From Fig. 3, the proposed fault-tolerant control FTC strategy consists of a four-leg VSI topology, a diagnostic algorithm generating the faulty IGBT detection time, a fault-tolerance algorithm providing the faulty phase isolation signals (S_{Ka}, S_{Kb}, S_{Kc}), and reconfiguration signals (S_{TRa}, S_{TRb}, S_{TRc}). The four-leg topology still allows the induction motor to operate with three phases under post-fault operation and does not require a change in the SVM-IFOC strategy or a new machine model.

During normal operation of the IM drive, the redundant r-leg is inactive, i.e., all switches TRx ($x = a, b, c$) are turned OFF.

Table 3. Isolation and reconfiguration signals of the proposed FTC block.

Types of OC faults	Signals for leg isolation S_{Ka}, S_{Kb}, S_{Kc}	Configuration signals $S_{TRa}, S_{TRb}, S_{TRc}$
T_1 or T_2 or (T_1 & T_2)	(0,1,1)	(1,0,0)
T_3 or T_4 or (T_3 & T_4)	(1,0,1)	(0,1,0)
T_5 or T_6 or (T_5 & T_6)	(1,1,0)	(0,0,1)

Table 4. Parameters of the three-phase induction motor.

Power P	1.5 kW	Rotor inductance L_r	0.61 H
Rated speed N	1400 rpm	Stator inductance L_s	0.39 H
Frequency f	50 Hz	Rotor resistance R_r	3.59
Line current I	6.3 A	Stator resistance R_s	5.43
Rated voltage V	380 V	Moment of inertia J	0.027 $kg.m^2$
Mutual inductance L_m	0.47 H	Pole pairs p	2

Consequently, the all-phase currents, as well as isolation and reconfiguration signals, are:

$$\begin{cases} i_a = I_P \sin\left(\omega_e t\right), \ i_b = I_P \sin\left(\omega_e t - 2\pi/3\right), \\ i_c = I_P \sin\left(\omega_e t + 2\pi/3\right), \ i_r = 0 \\ S_{Ka} = S_{Kb} = S_{Kc} = 1, \ S_{TRa} = S_{TRb} = S_{TRc} = 0 \end{cases} \quad (25)$$

When an OCF happens in a single- or double-switch of the VSI, the fault diagnosis algorithm identifies the faulty IGBT. Next, the fault-tolerant algorithm receives the diagnostic information and sets the appropriate isolation and reconfiguration signals. The control of extra switches T_7 and T_8 is ensured by the switching signals of the faulted leg. In the post-fault operation, signals for leg isolation and VSI reconfiguration are listed in Table 3:

4. RESEARCH RESULTS

A simulation model is built using MATLAB/Simulink software to validate the effectiveness of the suggested power switch OCF diagnostic method and FTC strategy. The main parameters of the induction motor used in the simulation are listed in Table 4. It is to highlight that the OCFs are simulated by detaching the gate pulse signal from the considered faulty switch. Also, the considered fault scenarios are open-circuit single- and double-switch faults (open-phase faults).

The induction motor closed-loop speed control is based on indirect field-oriented control (IFOC) with space vector modulation (SVM), as indicated in Fig. 4.
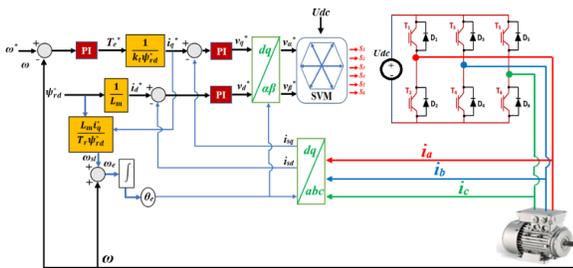

Fig. 4. Block diagram of SVM indirect field-oriented control strategy.

where ψ_{rd}^*, T_e^* are reference flux and reference torque, respectively, i_{sd}^*, i_{sq}^* are stator current components in the synchronous rotating frame. Whereas θe is the rotor flux angle, ω_{sl} is sleep frequency, and ω is the electrical speed. More details on the IM model, as well as the equations of the IFOC algorithm, are reported in [5].

4.1. IGBT open circuit faults diagnosis

A) Case 1: Single OCF results

Figs. 5, 6, and 7 show the results of speed, electromagnetic torque, motor currents, diagnosis variables, and fault flags for single OCF arising in the IGBT switches T_1, T_2, and T_3, respectively. The IM is driven at 1000 rpm and 50% of the rated load, i.e., 5 N.m.

As displayed in Fig. 5-(c), when OCF occurs at $t = 0.618$ sec in T_1 of the a-phase, the positive half-cycle of current i_a is lost. As a result, the diagnosis variable ηa quickly rises to almost 0.2, exceeding the adaptive threshold Th_{ad}. The other variables (ηb, ηc) converge to -0.12 and -0.10, respectively, as shown in Fig. 5-(d). Besides, the flag $IGBT_{12}$ grows to 1 at t = 0.6265 sec, as shown in Fig. 5-(e). Thus, it can be concluded that the T_1 OCF is detected after 8.5 msec, which is equivalent to 28.4% of the current fundamental period.
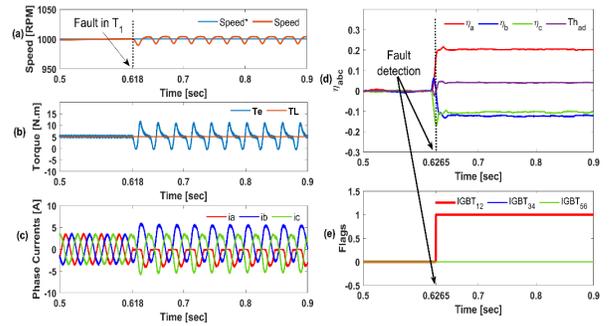

Fig. 5. Simulation results for an open-circuit fault in switch T1 (for 50% of the rated load and reference speed of 1000 r/min).
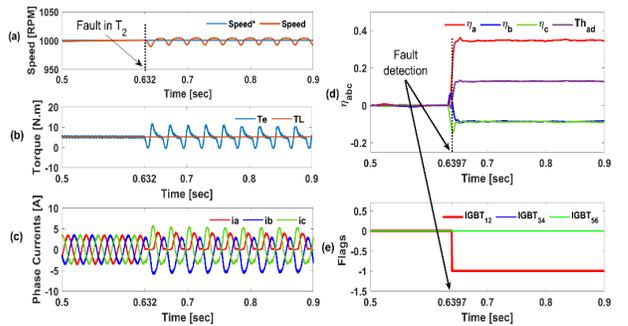

Fig. 6. Simulation results for an open-circuit fault in switch T2 (for 50% of the rated load and reference speed of 1000 r/min).

From Fig. 6-(c), it can be seen that the a-phase current only takes a positive half-cycle at t= 0.632 sec. As well, the diagnostic variables ηa, ηb, and ηc change rapidly and take new values different from zero (i.e., $\eta a = 0.34$, $\eta b = -0.09$, and $\eta c = -0.09$), as shown in Fig. 6-(d). Besides, the diagnostic flag $IGBT_{12}$ drops to -1 when ηa exceeds the threshold Th_{ad} at t = 0.6397 sec, while $IGBT_{34}$ and $IGBT_{56}$ remain zero, as indicated in Fig. 6-(e). According to Table 2, the diagnosis algorithm detects the T_2 OCF in 7.6 msec, corresponding to 25.5% of the current fundamental period.

As can be seen from Fig. 7-(c), when T_3 is OC at t= 0.656 sec, the b-phase current i_b converts from a sinusoidal cycle to a positive half-cycle, and the variable ηb rises rapidly and exceeds the threshold at t= 0.6647 sec. At this instant, the corresponding flag $IGBT_{34}$ steps from 0 to 1, as illustrated in Fig. 7-(e). Thus, the T_3 OCF is diagnosed after 8.7 msec (i.e., 29% of the current fundamental period).
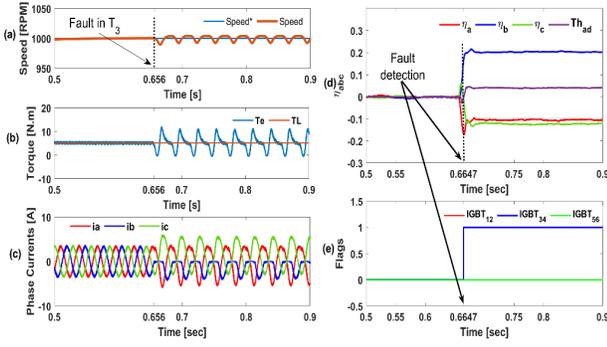
Fig. 7. Simulation results for an open-circuit fault in switch T3 (for 50% of the rated load and reference speed of 1000 r/min).

For the above fault scenarios, it can be seen that speed and torque are affected and exhibit ripples once the fault occurs, as shown in Figs. 5-(a, b), 6-(a, b), and 7-(a, b).

B) Case 2: OC double-switch fault results

Figs. 8 and 9 show the diagnosis results for scenarios of OC double switch faults in a-phase and b-phase, respectively. In Figs. 8-(c) and 9-(c), for (T_1, T_2) and (T_3, T_4) OCFs, respectively, both currents i_a and i_b become zero after the fault occurrence. In this instant, speed and electromagnetic torque undergo rapid ripples at a frequency equal to almost twice the current's frequency, as shown in Figs. 8-(a, b), and 9-(a, b).
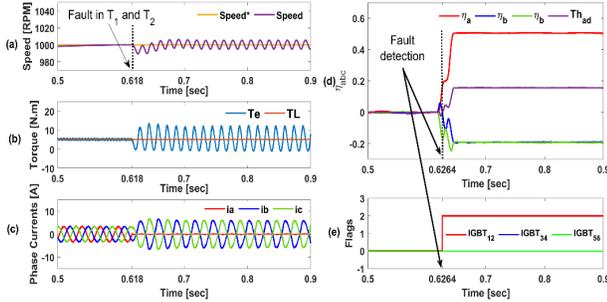

Fig. 8. Simulation results for an OCF of a-phase (T1+T2) (for 50% of the rated load and reference speed of 1000 r/min).
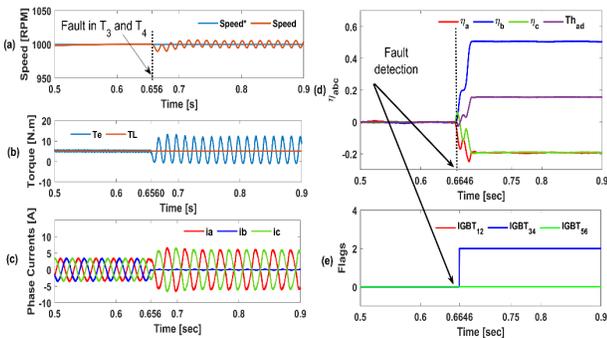

Fig. 9. Simulation results for an OCF of a-phase (T3+T4) (for 50% of the rated load and reference speed of 1000 r/min).

In Fig. 8, an OCF happens at t= 0.618 sec in both switches (T_1, T_2) of a-phase. As a result, the diagnosis variable ηa increases and reaches a value of 0.5, whereas the other ones $(\eta b, \eta c)$ of the healthy legs reach a value of -0.2, as shown in Fig. 8-(d). Once

the variable ηa of the failed leg exceeds the threshold Th_{ad} at t= 0.6264 sec, the fault flag $IGBT_{12}$ changes from 0 to 2, while $IGBT_{34}$ and $IGBT_{56}$ remain equal to zero, as presented in 8-(e). Hence, according to Table 2, the OC double-switch (T_1, T_2) fault is detected after 8.4 msec of the failure occurrence, namely within a time interval of about 28% of the current fundamental period.

Fig. 9-(d-e) illustrates the diagnosis results when an OC double switch fault happens in T_3 and T_4. As can be seen in Fig. 9-(e), the value of the fault flag $IGBT_{34}$ rises to 2 at t= 0.6646 sec, while $IGBT_{12}$ and $IGBT_{56}$ preserve zero, which means that the OCF occurs in the VSI b-phase. The FD algorithm takes 8.6 msec to detect the fault, which is equivalent to 28.6% of the current fundamental period.

4.2. Fault diagnosis method during a load torque transient

This part focuses on the robustness of the suggested diagnosis method against false alarms caused by load torque transients.
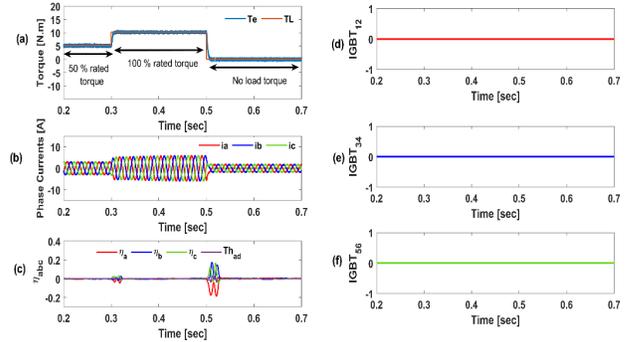

Fig. 10. Effectiveness of the proposed diagnosis method under load torque variations.

Fig. 10 includes the electromagnetic torque, speed, phase currents, diagnosis variables, and diagnosis flags during a load torque transient. The reference speed is set to 1300 rpm. As shown in Fig. 10-(a), the load changes at time t=0.3 sec from 50% to 100% of the rated torque value, then decreases at t=0.5 sec from 100% to 0% of the rated torque. Based on Fig. 10-(b), it is clear that the current's amplitudes increase and decrease with the load change.

As indicated in Fig. 10-(c), the diagnosis variables $(\eta a, \eta b, \eta c)$ present fluctuations at t=0.3 sec and t=0.5 sec; however, the diagnosis signatures for OCFs in Table 2 were not met. Thus, the diagnosis flags $(IGBT_{12}, IGBT_{34},$ and $IGBT_{56})$ remain equal to zero, as shown in Figs. 10-(d, e, f), indicating that the proposed FD method can resist load variations without generating false alarms.

4.3. Fault-tolerance control operation of induction motor drive

Fig. 11 illustrates the simulation results of the fault-tolerant control strategy against open-switch faults for an induction motor operating with a rotor speed of 1000 rpm and 50% of the rated torque. At the instant $tf = 0.656$ sec, an OCF in IGBT T_3 of b-phase occurs.

As displayed in Fig. 11-(a), the phase currents waveforms are sinusoidal before the fault. The positive b-phase current half period will drop to zero after the IGBT T3 OCF occurs. Additionally, it can be observed that when a fault occurs, both torque and speed exhibit ripples, as depicted in Figs. 11-(b) and Fig. 11-(c), respectively. Furthermore, the IM drive system returns to its normal state after the fault-tolerance control FTC strategy takes effect at t_{FTC}=0.756 sec by turning ON the TR_b and turning OFF Kb. Thus, torque and motor speed oscillations are eliminated, and the
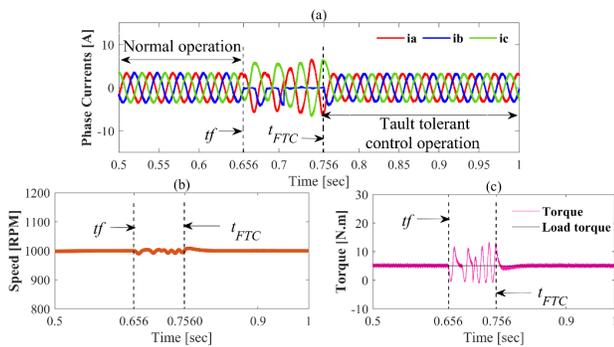
Fig. 11. Simulation results of fault tolerant control strategy applied to IM drive in case of OCF in T3 of b-phase with 1000 rpm and 5 N.m.
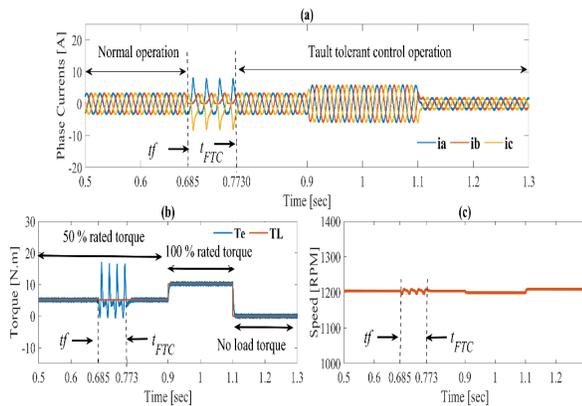

Fig. 12. Simulation results of fault tolerant control strategy in case of OCF in T4 with 1200 rpm and under load torque variations.

phase current waveforms become sinusoidal again. It should be mentioned that the faulty b-leg is isolated at t_{iso}=0.706 sec.

The response of the FTC was also evaluated under load torque variations, as shown in Fig. 12. At tf = 0.685 sec, an OCF happens in T_4. The IM runs at 1200 rpm, and two load changes are introduced, as shown in Fig. 12-(b). At t = 0.9 sec, the load steps from 50% to 100% of the rated torque, then at t=1.1 sec, it decreases from 100% to 0% of the rated torque, which results in an evident change of the currents, as shown in Fig. 12-(a). The FTC strategy is introduced at t_{FTC}=0.773 sec. Consequently, the OCF is effectively tolerated, and the oscillations in torque and speed are fully eliminated, as shown in Figs. 12-(b) and 12-(c). As visible from these findings, the proposed fault-tolerance IFOC strategy responds well to changes in load torque.

Table 5. Comparison between VSI open circuit fault diagnosis methods.

OCF diagnosis methods	Diagnosis speed: (%) of the phase currents fundamental period	Number of diagnosis variables	The studied faults
Suggested method	25 - 30%	01	single-IGBT and open-phase
Stator Current Analysis [17]	30 - 90%	02	multiple switches, single-IGBT
Fuzzy logic-based method [16]	200%	02	multiple switches, single-IGBT
Predictive current errors [21]	12 - 75%	02	multiple switches, single-IGBT
Reference current errors [12]	5 - 67%	02	multiple switches, single-IGBT
Probability density analysis [29]	100%	-	single-IGBT and open-phase
Fuzzy logic - current-based method [19]	45%	03	multiple switches, single-IGBT

4.4. Comparison with some open switch fault diagnosis methods

Table 5 stats a comparison between the suggested method and some current-based diagnosis methods outlined in the literature for detecting and identifying the OCFs in VSIs. The comparison indicators include the diagnostic speed, the number of diagnostic variables required, and the studied OCFs. The findings in Table 5 allow us to conclude that the suggested approach provides a quick diagnostic time (ranging from 25-30% of the fundamental period of motor currents). Besides, the proposed FD method requires only one FD variable.

5. CONCLUSION

In this article, a new fault-tolerance IFOC strategy for OCFs in an induction motor drive has been proposed and verified through simulation results. The findings show that the developed FD method offers a fast speed for diagnostics (within 25-30% of the phase current's fundamental period). Furthermore, the proposed FD approach does not require additional sensors and presents desirable robustness against false alarms caused by mechanical load variations. Moreover, it can be employed either in closed-loop or open-loop control techniques. To increase the fault tolerance capabilities of the IM drive system, a VSI topology with a redundant leg is used. The FT strategy does not need a change in vector controller (SVM-IFOC) and provides the same performance as a three-leg inverter; nevertheless, it consumes additional electronic components such as TRIACs and isolation switches.

The proposed FTC system can be extended to encompass all types of OCFs in the VSI and improved with experimental validation, which can be discussed in future work.

REFERENCES

[1] D. U. Campos-Delgado, J. A. Pecina-Sánchez, D. R. Espinoza-Trejo, and E. R. Arce-Santana, "Diagnosis of open-switch faults in variable speed drives by stator current analysis and pattern recognition," *IET Electr. Power Appl.*, vol. 7, no. 6, pp. 509–522, 2013.

[2] T. Chen, Y. Pan, and Z. Xiong, "Fault diagnosis scheme for single and simultaneous open-circuit faults of voltage-source inverters on the basis of fault online simulation," *J. Power Electron.*, vol. 21, no. 2, pp. 384–395, 2021.

[3] Y. Zhang, "Current behavior-based open-switch fault on-line diagnosis of inverters in pmsm drive systems," *Meas.*, vol. 202, p. 111810, 2022.

[4] C. N. Ibem, M. E. Farrag, A. A. Aboushady, and S. M. Dabour, "Multiple open switch fault diagnosis of three phase voltage source inverter using ensemble bagged tree machine learning technique," *IEEE Access*, 2023.

[5] H. Zaimen, A. Rezig, and S. Touati, "A new detection method of igbts open-circuit faults in an induction motor drive," *Turk. J. Comput. Math. Educ.*, vol. 13, no. 2, pp. 748–760, 2022.

[6] P. Sobanski and T. Orlowska-Kowalska, "Faults diagnosis and control in a low-cost fault-tolerant induction motor drive system," *Math. Comput. Simul.*, vol. 131, pp. 217–233, 2017.

[7] T. Chen and Y. Pan, "A novel diagnostic method for multiple open-circuit faults of voltage-source inverters based on output line voltage residuals analysis," *IEEE Trans. Circuits Syst. II Express Briefs*, vol. 68, no. 4, pp. 1343–1347, 2020.

[8] A. Mendes and A. M. Cardoso, "Fault diagnosis in a rectifier-inverter system used in variable speed ac drives by the average current park's vector approach," in *Eur. Power Electron. Conf.*, pp. 1–9, 1999.

[9] K. Rothenhagen and F. W. Fuchs, "Performance of diagnosis methods for igbt open circuit faults in three phase voltage source inverters for ac variable speed drives," in *2005 Eur. Conf. Power Electron. Appl.*, pp. 10–pp, IEEE, 2005.

[10] K. Rothenhagen and F. W. Fuchs, "Performance of diagnosis methods for igbt open circuit faults in voltage source active rectifiers," in *2004 IEEE 35th Annu. Power Electron. Specialists Conf. (IEEE Cat. No. 04CH37551)*, vol. 6, pp. 4348–4354, IEEE, 2004.

[11] M. Trabelsi, M. Boussak, and M. Gossa, "Multiple igbts open circuit faults diagnosis in voltage source inverter fed induction motor using modified slope method," in *The XIX Int. Conf. Electr. Mach.-ICEM 2010*, pp. 1–6, IEEE, 2010.

[12] J. O. Estima and A. J. M. Cardoso, "A new algorithm for real-time multiple open-circuit fault diagnosis in voltage-fed pwm motor drives by the reference current errors," *IEEE Trans. Ind. Electron.*, vol. 60, no. 8, pp. 3496–3505, 2012.

[13] J. O. Estima and A. J. M. Cardoso, "A new approach for real-time multiple open-circuit fault diagnosis in voltage-source inverters," *IEEE Trans. Ind. Appl.*, vol. 47, no. 6, pp. 2487–2494, 2011.

[14] R. Peuget, S. Courtine, and J.-P. Rognon, "Fault detection and isolation on a pwm inverter by knowledge-based model," *IEEE Trans. Ind. Appl.*, vol. 34, no. 6, pp. 1318–1326, 1998.

[15] K. Wang, X. Jiang, S. Wang, and Z. Han, "Power switch open circuit fault diagnosis strategy for novel fault-tolerant electric drive system based on fuzzy logic," *Energy Rep.*, vol. 8, pp. 914–921, 2022.

[16] H. Yan, Y. Xu, F. Cai, H. Zhang, W. Zhao, and C. Gerada, "Pwm-vsi fault diagnosis for a pmsm drive based on the fuzzy logic approach," *IEEE Trans. Power Electron.*, vol. 34, no. 1, pp. 759–768, 2018.

[17] S. K. El Khil, I. Jlassi, A. J. M. Cardoso, J. O. Estima, and N. Mrabet-Bellaaj, "Diagnosis of open-switch and current sensor faults in pmsm drives through stator current analysis," *IEEE Trans. Ind. Appl.*, vol. 55, no. 6, pp. 5925–5937, 2019.

[18] H. Yan, Y. Xu, J. Zou, Y. Fang, and F. Cai, "A novel open-circuit fault diagnosis method for voltage source inverters with a single current sensor," *IEEE Trans. Power Electron.*, vol. 33, no. 10, pp. 8775–8786, 2017.

[19] M. A. Zdiri, M. Ben Ammar, F. Ben Salem, and H. Hadj Abdallah, "Pwm-vsi diagnostic and reconfiguration method based on fuzzy logic approach for sstpi-fed im drives under igbt ocfs," *Math. Probl. Eng.*, vol. 2021, pp. 1–18, 2021.

[20] R. Manikandan, S. Raghu, and R. R. Singh, "An improved open switch fault diagnosis strategy for variable speed drives," in *2022 IEEE Int. Conf. Power Electron. Smart Grid Renewable Energy (PESGRE)*, pp. 1–6, IEEE, 2022.

[21] B. Gmati, I. Jlassi, S. Khojet El Khil, and A. J. Marques Cardoso, "Open-switch fault diagnosis in voltage source inverters of pmsm drives using predictive current errors and fuzzy logic approach," *IET Power Electron.*, vol. 14, no. 6, pp. 1059–1072, 2021.

[22] Z. Jian-Jian, C. Yong, C. Zhang-Yong, and Z. Anjian, "Open-switch fault diagnosis method in voltage-source inverters based on phase currents," *IEEE Access*, vol. 7, pp. 63619–63625, 2019.

[23] R. Tabasian, M. Ghanbari, A. Esmaeli, and M. Jannati, "Control of three-phase induction machine drives during open-circuit fault: A review," *IETE J. Res.*, vol. 68, no. 4, pp. 2622–2639, 2022.

[24] M. Shabandokht-Zarami, M. Ghanbari, E. Alibeiki, and M. Jannati, "An improved foc strategy for speed control of induction motor drives under an open-phase fault using genetic algorithm," *J. Oper. Autom. Power Eng.*, vol. 10, no. 1, pp. 80–89, 2022.

[25] M. Nikpayam, M. Ghanbari, A. Esmaeli, and M. Jannati, "Vector control methods for star-connected three-phase induction motor drives under the open-phase failure," *J. Oper. Autom. Power Eng.*, vol. 10, no. 2, pp. 155–164, 2022.

[26] E. Z. Salem, A. Haitham Z, A.-G. Saad F, and M. M. Elkholy, "Open gate fault diagnosis and tolerant for voltage source inverter fed speed sensorless induction motor drive," *Int. J. Electron.*, vol. 107, no. 11, pp. 1754–1772, 2020.

[27] R. Bolbolnia, K. Abbaszadeh, and M. Nasiri, "Diagnosis and fault-tolerant control of six-phase wind turbine under multiple open-switch faults," *Math. Probl. Eng.*, vol. 2021, pp. 1–16, 2021.

[28] B. D. E. Cherif, A. Djerioui, S. Zeghlache, S. Seninete, and A. Tamer, "Indirect vector controlled of an induction motor using h current controller for igbt open circuit fault compensation," *Int. Trans. Electr. Energy Syst.*, vol. 30, no. 10, p. e12540, 2020.

[29] D. Zhou, Y. Li, J. Zhao, F. Wu, and H. Luo, "An embedded closed-loop fault-tolerant control scheme for nonredundant vsi-fed induction motor drives," *IEEE Trans. Power Electron.*, vol. 32, no. 5, pp. 3731–3740, 2016.